Morphology Changes and Mechanistic Aspects of the Electrochemically-Induced Reversible Solid−Solid Transformation of Microcrystalline TCNQ into $Co[TCNQ]_2$-Based Materials (TCNQ = 7,7,8,8-Tetracyanoquinodimethane)

Ayman Nafady,[†] Anthony P. O'Mullane,[†] Alan M. Bond,*[,†] and Aaron K. Neufeld[‡]

School of Chemistry, Monash University, P.O. Box 23, Victoria 3800, Australia and BlueScope Steel Limited, Coatings Research, P.O. Box 202, Old Port Road, Port Kembla NSW 2505, Australia

Received April 13, 2006. Revised Manuscript Received June 29, 2006

The chemically reversible solid−solid phase transformation of a TCNQ-modified glassy carbon, indium tin oxide, or metal electrode into $Co[TCNQ]_2(H_2O)_2$ material in the presence of $Co^{2+}_{(aq)}$ containing electrolytes has been induced and monitored electrochemically. Voltammetric data reveal that the TCNQ/$Co[TCNQ]_2(H_2O)_2$ interconversion process is independent of electrode material and identity of cobalt electrolyte anion. However, a marked dependence on electrolyte concentration, scan rate, and method of electrode modification (drop casting or mechanical attachment) is found. Cyclic voltammetric and double potential step chronoamperometric measurements confirm that formation of $Co[TCNQ]_2(H_2O)_2$ occurs through a rate-determining nucleation and growth process that initially involves incorporation of $Co^{2+}_{(aq)}$ ions into the reduced TCNQ crystal lattice at the TCNQ|electrode|electrolyte interface. Similarly, the reverse (oxidation) process, which involves transformation of solid $Co[TCNQ]_2(H_2O)_2$ back to parent TCNQ crystals, also is controlled by nucleation−growth kinetics. The overall chemically reversible process that represents this transformation is described by the reaction: $2TCNQ^0_{(s)} + 2e^- + Co^{2+}_{(aq)} + 2H_2O \rightleftharpoons [Co(TCNQ)_2(H_2O)_2]_{(s)}$. Ex situ SEM images illustrated that this reversible TCNQ/$Co[TCNQ]_2(H_2O)_2$ conversion process is accompanied by drastic size and morphology changes in the parent solid TCNQ. In addition, different sizes of needle-shaped nanorod/nanowire crystals of $Co[TCNQ]_2(H_2O)_2$ are formed depending on the method of surface immobilization.

Introduction

The properties of TCNQ-based molecular materials (TCNQ = 7,7,8,8-tetracyanoquinodimethane, structure 1) such as charge-transfer salts, organometallic compounds, and coordination polymers have generated a great deal of interest over the past four decades,[1−15] particularly with respect to their use in storage and light emitting devices, catalysis, and sensing applications.[16−24]

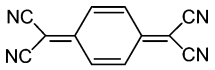

Structure 1

The continuing interest is illustrated in the case of CuTCNQ, where the structural, electronic, optical, and conducting properties of this transition-metal charge-transfer complex have received considerable recent attention.[25−28] For example, it is now known that CuTCNQ exists in two distinct

* To whom correspondence should be addressed. Fax: 613-9905-4597. E-mail: Alan.Bond@sci.monash.edu.au.
† Monash University.
‡ BlueScope Steel Limited.

(1) Acker, D. S.; Harder, R. J.; Hertler, W. R.; Mahler, W.; Melby, L. R.; Benson, R. E.; Mochel, W. E. *J. Am. Chem. Soc.* **1960**, *82*, 6408.
(2) Torrance, J. B.; Scott, B. A.; Kaufman, F. B. *Solid State Commun.* **1975**, *17*, 1369.
(3) Reis, A. H., Jr.; Preston, L. D.; Williams, J. M.; Peterson, S. W.; Candela, G. A.; Swartzendruber, L. J.; Miller, J. S. *J. Am. Chem. Soc.* **1979**, *101*, 2756.
(4) Poehler, T. O.; Potember, R. S.; Hoffman, R.; Benson, R. C. *Mol. Cryst. Liq. Cryst.* **1984**, *107*, 91.
(5) Ward, M. D.; Johnson, D. C. *Inorg. Chem.* **1987**, *26*, 4213.
(6) Miller, J. S.; Epstein, A. J.; Reiff, W. M. *Chem. Rev.* **1988**, *88*, 201.
(7) O'Hare, D.; Ward, M. D.; Miller, J. S. *Chem. Mater.* **1990**, *2*, 758.
(8) Bell, S. E.; Field, J. S.; Haines, R. J.; Sundermeyer, J. *J. Organomet. Chem.* **1992**, *427*, C1.
(9) Dvorak, M. A.; Li, S.; Ward, M. D. *Chem. Mater.* **1994**, *6*, 1386.
(10) Broderick, W. E.; Eichhorn, D. M.; Liu, X.; Toscano, P. J.; Owens, S. M.; Hoffman, B. M. *J. Am. Chem. Soc.* **1995**, *117*, 3641.
(11) Fortin, D.; Drouin, M.; Harvey, P. D. *J. Am. Chem. Soc.* **1998**, *120*, 5351.
(12) Pokhodnya, K. I.; Petersen, N.; Miller, J. S. *Inorg. Chem.* **2002**, *41*, 1996.
(13) Chi, X.; Besnard, C.; Thorsmolle, V. K.; Butko, V. Y.; Taylor, A. J.; Siegrist, T.; Ramirez, A. P. *Chem. Mater.* **2004**, *16*, 5751.
(14) Morita, Y.; Murata, T.; Fukui, K.; Yamada, S.; Sato, K.; Shiomi, D.; Takui, T.; Kitagawa, H.; Yamochi, H.; Saito, G.; Nakasuji, K. *J. Org. Chem.* **2005**, *70*, 2739.
(15) Cea, P.; Martin, S.; Villares, A.; Moebius, D.; Lopez, M. C. *J. Phys. Chem. B* **2006,** *110*, 963.
(16) Wheland, R. C.; Gillson, J. L. *J. Am. Chem. Soc.* **1976**, *98*, 3916.
(17) Kathirgamanathan, P.; Rosseinsky, D. R. *J. Chem. Soc., Chem. Commun.* **1980**, 839.
(18) Bolinger, C. M.; Darkwa, J.; Gammie, G.; Gammon, S. D.; Lyding, J. W.; Rauchfuss, T. B.; Wilson, S. R. *Organometallics* **1986**, *5*, 2386.
(19) Kulys, J.; Drungiliene, A. *Electroanalysis* **1991**, *3*, 209.
(20) Murthy, A. S. N.; Anita, G. R. L. *Anal. Chim. Acta* **1994**, *289*, 43.
(21) Wooster, T. J.; Bond, A. M.; Honeychurch, M. J. *Anal. Chem.* **2003**, *75*, 586.
(22) Wooster, T. J.; Bond, A. M. *Analyst* **2003**, *128*, 1386.
(23) Okamoto, T.; Kozaki, M.; Doe, M.; Uchida, M.; Wang, G.; Okada, K. *Chem. Mater.* **2005**, *17*, 5504.
(24) Mueller, R.; De Jonge, S.; Myny, K.; Wouters, D. J.; Genoe, J.; Heremans, P. *Solid State Electron.* **2006**, *50*, 601.
(25) Heintz, R. A.; Zhao, H.; Ouyang, X.; Grandinetti, G.; Cowen, J.; Dunbar, K. R. *Inorg. Chem.* **1999**, *38*, 144.

10.1021/cm060852j CCC: $33.50
Published on Web 08/12/2006

crystalline phases[25,28] (I and II), with phase I being significantly more conductive, which suggests a potential use as a material for optical data storage in molecular devices.[24] In contrast, knowledge concerning the conceptually and structurally related binary $M[TCNQ]_2(S)$ complexes, where M represents a first-row transition metal (Mn, Fe, Co, Ni) and S is a coordinating solvent, is relatively underdeveloped.[29] The initial report of such compounds appears to be the 1962 paper by Melby and co-workers,[30] who synthesized a series of $M[TCNQ]_2 \cdot 3H_2O$ (M = Mn, Fe, Co, Ni) complexes. Recently, Dunbar et al. reported materials having the general formula $M[TCNQ]_2(S)_2$, where S is methanol or water solvates.[31,32] These solvated materials together with their nonsolvated forms[33,34] have been shown to exhibit interesting magnetic properties.[31−34] Most research activity on $M[TCNQ]_2$-based materials, therefore, has been focused on probing their structural, magnetic, and conducting properties.[17,29,31−35]

In this contribution, via an extension of methodologies developed for CuTCNQ investigations,[26] we offer new insights into the mechanism as well as spectroscopic and microscopic characterization of the reversible solid−solid transformation of TCNQ into $Co[TCNQ]_2(H_2O)_2$ material that has been induced electrochemically via reduction of solid TCNQ in the presence of $Co^{2+}_{(aq)}$ electrolyte solutions. The key experimental approach employed to probe this reversible interconversion involves voltammetric studies at glassy carbon (GC) or indium tin oxide (ITO) working electrodes modified with solid TCNQ by either drop-casting or mechanical attachment methods.[36] The influence of electrode material, electrolyte identity, and concentration on the redox process has been explored in detail. With the aid of images obtained by scanning electron microscopy (SEM), changes in both morphology and particle size of TCNQ that accompany its transformation into $Co[TCNQ]_2(H_2O)_2$ material are detected. XRD data give evidence that the electrochemically produced $Co[TCNQ]_2(H_2O)_2$ complex exists only in one crystalline phase, consistent with that previously prepared via chemical methods.[31]

Experimental Section

Materials and Synthesis of $Co[TCNQ]_2(H_2O)_2$. Analytical-grade cobalt(II) salts obtained from various commercial sources and TCNQ (98%) purchased from Aldrich were used as received. Acetonitrile (HPLC, Omnisolv) was used to prepare stock (10 mM) solutions of TCNQ. $Co[TCNQ]_2(H_2O)_2$ was chemically synthesized and characterized following the procedures described by Zhao et al.[31]

Electrochemical Instrumentation and Procedures. Aqueous electrolytes were prepared using purified water obtained from a Millipore System (resistivity 18.2 MΩ cm). Voltammetric experiments were conducted at 293 ± 2 K with an Autolab PGSTAT100 (ECO-Chemie) electrochemical workstation using a standard three-electrode electrochemical cell configuration. The working electrodes used were glassy carbon disk (3 mm diameter, IJ Cambria), gold and platinum (1.6 mm diameter, Bioanalytical Systems), or 10 Ω/sq (as quoted by manufacturer) glass covered indium tin oxide (ITO) (Prazisions Glas and Optik GmbH) typically having an area of 0.06−0.09 cm^2. All electrodes, except for ITO, were polished with a 0.3 μm alumina slurry on Microcloth polishing cloth, rinsed copiously with deionized water, and then sonicated in an ultrasonic bath for 5 min prior to use. In the case of ITO electrodes, they were cleaned by sonication for 5 min in both acetone (MERCK) and 2-propanol (BDH) solutions, respectively, and then dried under nitrogen. The reference electrode was an aqueous Ag/AgCl (3 M KCl) from Bioanalytical Systems, and the counter electrode was made from platinum mesh. Nitrogen gas was used to sparge the aqueous solutions in which chemically modified electrodes were placed, and a flow of this gas was maintained above the solution during the course of electrochemical experiments.

Modification of Electrode Surface. Two methods were used to immobilize TCNQ onto the GC, ITO, or metal electrodes. In the first method of modification, namely, drop casting, the working electrodes were immersed in a 10 mM acetonitrile solution of TCNQ, after which the electrode was removed from the solution and suspended face down, thereby allowing the droplet of acetonitrile containing the dissolved TCNQ to evaporate. In the case of the ITO electrode, the surface was modified by applying a few droplets of the 10 mM TCNQ−acetonitrile solution. These procedures result in formation of an array of regularly spaced TCNQ microcrystals having a rhombic shape. A representative SEM image of a TCNQ single crystal produced by this method is illustrated (vide infra) in the SEM section (Figure 6a).

In the second approach, mechanical attachment, a small amount of solid TCNQ was placed on a glass substrate over which the electrode was rubbed, thus causing the solid to adhere to the surface. Figure 7a (in the SEM section) shows a typical SEM image of an ITO electrode modified in this manner with solid TCNQ. It is clear from this image that mechanically attached TCNQ solid adheres to the electrode surface to give a compressed layered format with a variety of particle sizes and shapes. The mechanical attachment method leads to immobilization of a greater quantity of TCNQ material on the electrode surface. However, both methods produce stable films of adhered TCNQ suitable for voltammetric, spectroscopic, and SEM characterization as shown below.

Other Instrumentation. Infrared (IR) spectra of chemically synthesized $Co[TCNQ]_2(H_2O)_2$ complex were recorded as KBr disks using a Bruker Equinox 55 spectrometer and an IR Scope II infrared microscope. IR spectra of the products formed on the surface of the GC or ITO electrodes during the course of voltammetric or controlled potential electrolysis experiments were obtained as reflectance spectra with the aid of an inverted Praying Mantis (Harrick Scientific) diffuse reflectance optical accessory. Typically, after removal from the electrochemical cell, the electrodes containing the solid materials were gently washed by immersing them in deionized water, dried under a stream of nitrogen, and then mounted in a collar for downward positioning, thereby ensuring that the surface of the electrode was in the focal plane of the incident

(26) Neufeld, A. K.; Madsen, I.; Bond, A. M.; Hogan, C. F. *Chem. Mater.* **2003**, *15*, 3573.
(27) Neufeld, A. K.; O'Mullane, A. P.; Bond, A. M. *J. Am. Chem. Soc.* **2005**, *127*, 13846.
(28) O'Mullane, A. P.; Neufeld, A. K.; Bond, A. M. *Anal. Chem.* **2005**, *77*, 5447.
(29) Siedle, A. R.; Candela, G. A.; Finnegan, T. F. *Inorg. Chim. Acta* **1979**, *35*, 125.
(30) Melby, L. R.; Harder, R. J.; Hertler, W. R.; Mahler, W.; Benson, R. E.; Mochel, W. E. *J. Am. Chem. Soc.* **1962**, *84*, 3374.
(31) Zhao, H.; Heintz, R. A.; Ouyang, X.; Dunbar, K. R.; Campana, C. F.; Rogers, R. D. *Chem. Mater.* **1999**, *11*, 736.
(32) Zhao, H.; Heintz, R. A.; Dunbar, K. R.; Rogers, R. *J. Am. Chem. Soc.* **1996**, *118*, 12844.
(33) Clérac, R.; O'Kane, S.; Cowen, J.; Ouyang, X.; Heintz, R.; Zhao, H.; Bazile, M. J.; Dunbar, K. R. *Chem. Mater.* **2003**, *15*, 1840.
(34) Vickers, E. B.; Giles, I. D.; Miller, J. S. *Chem. Mater.* **2005**, *17*, 1667.
(35) De Caro, D.; Basso-Bert, M.; Casellas, H.; Elgaddari, M.; Savy, J.-P.; Lamere, J.-F.; Bachelier, A.; Faulmann, C.; Malfant, I.; Etienne, M.; Valade, L. *C. R. Chimie* **2005**, *8*, 1156.
(36) Hogan, C. F.; Bond, A. M.; Neufeld, A. K.; Connelly, N. G.; Liamas-Rey, E. *J. Phys. Chem. A* **2003**, *107*, 1274.

infrared beam. Scanning electron micrographs (SEM) of $Co[TCNQ]_2(H_2O)_2$ electrochemically synthesized from TCNQ-modified ITO electrodes were obtained with a Philips XL30 field emission gun scanning electron microscope (FEGSEM) using both secondary (SE) and backscatter (BSE) imaging modes with accelerating voltages between 2 and 5 keV. Elements present in these materials were determined by energy-dispersive X-ray spectra obtained with an Oxford Link EDAX data analysis system. Powder X-ray diffraction data were obtained using a Phillips 1729 X-ray diffractrometer (XRD) with Cu Kα radiation in the range from 5° to 50° 2θ in steps of 0.02° with a counting time of 2 s $step^{-1}$.

Results and Discussion

I. Voltammetric Characterization of the Chemically Reversible TCNQ/$Co[TCNQ]_2(H_2O)_2$ Solid−Solid Redox Transformation. *I.A. Voltammetric Behavior of Solid TCNQ in the Presence of $Co^{2+}_{(aq)}$ Electrolyte.* Since reduction of Co^{2+} to Co (metal) in aqueous solutions occurs at a far more negative value than for reduction of TCNQ, the latter can be selectively reduced to the corresponding monoanion radical, $[TCNQ]^-$, in the presence of divalent cobalt cations. Consequently, cyclic voltammograms of TCNQ-modified GC electrodes (via either drop casting or mechanical attachment) obtained from scanning the potential over the range from 0.5 to −0.05 V vs Ag/AgCl must involve reduction of immobilized TCNQ and not reduction of $Co^{2+}_{(aq)}$. Although the initial scans (Figure 1a) obtained at electrodes modified with TCNQ via the drop-casting method are complex, they reveal the onset of faradaic reduction current when 0.1 M $Co^{2+}_{(aq)}$ is present in solution at ∼0.012 V in the first sweep when the potential is scanned at a rate of 0.02 V s^{-1} in the negative direction from 0.5 to −0.05 V. On the reverse sweep, in the positive potential direction, the reduction current initially decreases and then slightly increases at a potential of approximately 0 V. This leads to current crossover with the initial reduction current at a potential of about 0.03 V, after which the current again decreases and reaches a zero current value at 0.11 V. At even more positive potentials an anodic current is detected which gradually increases until the oxidation peak potential (E_p^{ox}) is reached at 0.26 V. Observation of current loops in the initial cycle (Figure 1a) is indicative of nucleation and growth processes.[26,37−39] On cycling the potential, the voltammograms progressively become more reproducible and from the third cycle onward the shapes and peak potentials become almost independent of the number of cycles as illustrated in Figure 1a.

Most of the initial complexity observed when the electrode surface is modified via the drop-cast method is obviated when the working electrode is modified by mechanical attachment of solid TCNQ. In this method of surface modification, after the first cycle of the potential, reproducible cyclic voltammograms having sharp, well-separated, and symmetrical oxidation and reduction components are obtained (Figure 1b) when the electrode is in contact with 0.1 M $Co^{2+}_{(aq)}$. As can be seen from this figure, the fifth redox cycle exhibits a large

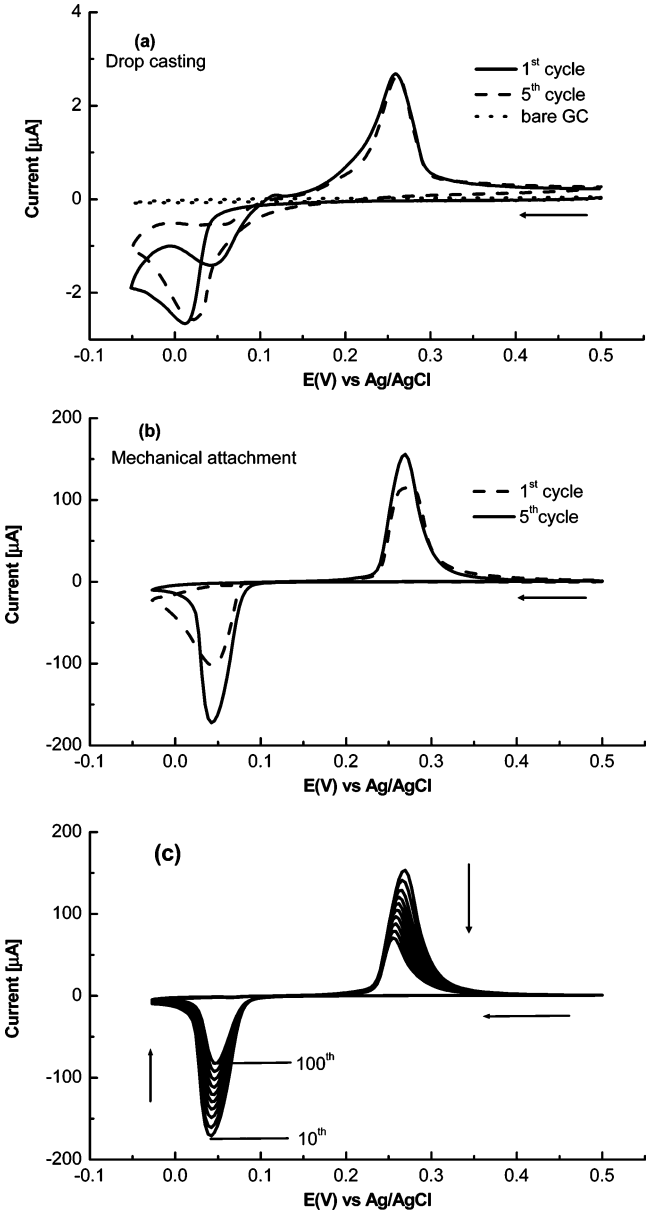

Figure 1. (a) Cyclic voltammograms at a scan rate of 0.02 V s^{-1} at bare (• • •) and drop-cast TCNQ-modified GC disk electrode for the first (—) and fifth (- - -) cycle of potential in contact with 0.1 M $Co(ClO_4)_2 \cdot 6H_2O_{(aq)}$ electrolyte. (b) As in a but with a GC electrode modified with TCNQ via the mechanical attachment method. (c) As in b but for the 10−100th cycle of the potential from 0.5 to −0.05 V, showing every 10th cycle.

peak separation ($\Delta E_p = E_p^{ox-red}$) or 'inert zone' of 0.23 V, which is characteristic for a wide range of solid-state voltammetric processes and consistent with those measured for MTCNQ systems of Group I cations (M = Na, Cs)[40] as well as the thermodynamically favored CuTCNQ phase II.[26] In addition, the peak width at half-height ($W_{1/2}$) of the reduction and oxidation waves is narrow (42 and 34 mV, respectively). The simplest process that can be proposed to represent the voltammetry would be the one described in eq 1.

$$2[TCNQ]_{(s,GC)} + Co^{2+}_{(aq)} + 2e^- + 2H_2O \rightleftharpoons Co[(TCNQ)_2(H_2O)_2]_{(s,GC)} \quad (1)$$

Apparently, ingress and egress of $Co^{2+}_{(aq)}$ ions occur more readily in the smaller sized mechanically attached crystals.

(37) Fletcher, S.; Halliday, C. S.; Gates, D.; Westcott, M.; Lwin, T.; Nelson, G. *J. Electroanal. Chem.* **1983**, *159*, 267−285.
(38) Bond, A. M.; Fletcher, S.; Marken, F.; Shaw, S. J.; Symons, P. G. *J. Chem. Soc., Faraday Trans.* **1996**, *92*, 3925.
(39) Suárez, M. F.; Marken, F.; Compton, R. G.; Bond, A. M.; Miao, W.; Raston, C. L. *J. Phys. Chem. B* **1999**, *103*, 5637.
(40) Bond, A.; Symons, P. G.; Fletcher, S. *Analyst* **1998**, *123*, 1891.

In the larger crystals produced by the drop-casting method (vide infra) fragmentation into smaller sized particles may occur during the initial cycles of the potential to eventually generate crystals of a size akin to those initially present in the mechanically attached method.

Despite the large peak potential separation of the reduction and oxidation components, chemical reversibility is observed upon extensive cycling of the potential. For example, the magnitude of the charge associated with the reduction component of the fifth cycle in Figure 1b, $Q_{red} = 3.83 \pm 0.23 \times 10^{-4}$ C, is, within experimental error, the same as that passed in the oxidation component during the reverse scan of the same cycle, $Q_{ox} = 3.86 \pm 0.20 \times 10^{-4}$ C.

The peak heights become slightly attenuated upon extensive cycling of the potential as illustrated in Figure 1c. Table 1 summarizes the voltammetric parameters obtained when the potential was cycled 100 times over the range from 0.5 to −0.05 V. The decrease in peak height as a function of the number of cycles is probably due to slow dissolution of TCNQ microcrystals[40] and electrochemically generated $Co[TCNQ]_2$-based material in aqueous media.[33] Moreover, the anticipated decrease in size of TCNQ crystals and change in morphology as a result of the redox transformation may increase the rate of material loss from the electrode surface upon repetitive cycling of the potential. Factors most likely to affect the $TCNQ/Co[TCNQ]_2(H_2O)_2$ conversion and $Co[TCNQ]_2(H_2O)_2$ dissolution (eq 2) processes include electrolyte identity, concentration, scan rate, and electrode material (see later discussion).

$$Co[TCNQ]_2(H_2O)_{2(S)} \rightarrow Co^{2+}{}_{(aq)} + 2TCNQ^-{}_{(aq)} + 2H_2O \quad (2)$$

The fact that only one oxidation wave is observed upon extensive cycling of the potential over the range from 0.5 to −0.05 V (see Figure 1c) suggests formation of only a single phase of $Co[TCNQ]_2$-based material. In contrast, electrosynthesis of CuTCNQ analogue, from aqueous solution, has given rise to two redox processes involving formation of the kinetically and thermodynamically favored phases I and II, respectively,[26] as shown by eqs 3 and 4.

$$TCNQ^0{}_{(s)} + Cu^{2+}{}_{(aq)} + 2e^- \rightleftharpoons Cu(TCNQ)_{(phase\ I)} \quad (3)$$

$$TCNQ^0{}_{(s)} + Cu^{2+}{}_{(aq)} + 2e^- \rightleftharpoons Cu(TCNQ)_{(phase\ II)} \quad (4)$$

I.B. Role of Electrode Material. Voltammetric characteristics obtained from TCNQ-modified 3 mm diameter glassy carbon, 1.6 mm platinum, 1.6 mm gold, and 0.09 cm^2 indium tin oxide (ITO) electrodes in contact with 0.1 M $Co(ClO_4)_{2(aq)}$ (Figure SM1 in Supporting Information and Table 2) were almost identical after the voltammetric steady state described above was achieved within about five cycles of the potential. This indicates that the underlying electrode material has no significant effect on the voltammetry of immobilized TCNQ microcrystals, thereby suggesting that rate-determining nucleation−growth reactions may occur within the bulk solid and/or at the surface of TCNQ microcrystals.

I.C. Role of Electrolyte Anion. Voltammetric parameters related to the potential and wave shape (E_p^{red}, $W_{1/2}{}^{red}$ and E_p^{ox}, $W_{1/2}{}^{ox}$) obtained for TCNQ microcrystals immobilized onto a GC electrode via mechanical attachment in the presence of 0.1 M aqueous solutions of $CoCl_2 \cdot 6H_2O$, $CoBr_2 \cdot H_2O$, $Co(NO_3)_2 \cdot 6H_2O$, $Co(ClO_4)_2 \cdot 6H_2O$, and $CoSO_4 \cdot 7H_2O$ show only a small dependence on the identity of the anion (Figure 2 and Table 3). This suggests that the electrolyte anions play no important role on the kinetics of solid−solid phase transformation. Moreover, the relatively constant ΔE_p and E_m values imply that the nucleation−growth process predominantly only involves the incorporation and exclusion of Co^{2+} ions into/from the lattice of TCNQ microcrystals. However, from the dissolution viewpoint (rate of attenuation of voltammetric peak currents with increasing number of cycles of potential) electrolytes containing ClO_4^- and NO_3^- anions gave the sharpest and most persistent voltammograms. Therefore, these two electrolyte anions have been preferably used in electrochemical synthesis studies aimed at characterization of $Co[TCNQ]_2$-based materials (see section II).

I.D. Effect of Electrolyte Concentration. Inspection of Figure 3a reveals that cyclic voltammograms for the $TCNQ/Co[TCNQ]_2(H_2O)_2$ conversion process significantly depend on the concentration of $Co^{2+}{}_{(aq)}$. Consistent with previously investigated MTCNQ systems,[26,40] the sharpest voltammetric wave shape with the highest peak current is obtained for a $Co^{2+}{}_{(aq)}$ electrolyte concentration of 0.1 M (see Figure 3a). Moreover, the attenuation rate with potential cycling is smaller than in other concentration regimes. At 0.001 M $Co^{2+}{}_{(aq)}$ concentration, severe broadening of the oxidation and reduction peaks and a large increase in peak separation

Table 1. Voltammetric Parameters[a] Obtained at a Scan Rate of 0.02 V s^{-1} with a TCNQ-Modified GC Electrode (Mechanical Attachment) Immersed in 0.1 M $Co(ClO_4)_{2(aq)}$ as a Function of the Number of Cycles of the Potential

cycle no.	Q_{red} (μC)	E_p^{red} (V)	$W_{1/2}{}^{red}$ (V)	Q_{ox} (μC)	E_p^{ox} (V)	$W_{1/2}{}^{ox}$ (V)	E_m (V)	ΔE_p^{ox-red} (V)
10	376	0.042	0.038	379	0.268	0.040	0.155	0.226
20	355	0.042	0.038	360	0.266	0.039	0.154	0.224
30	327	0.042	0.037	332	0.264	0.039	0.153	0.222
40	302	0.043	0.037	307	0.262	0.038	0.153	0.219
50	279	0.044	0.036	285	0.261	0.037	0.153	0.217
60	257	0.044	0.035	262	0.260	0.035	0.152	0.216
70	234	0.045	0.034	238	0.258	0.034	0.152	0.213
80	211	0.046	0.033	215	0.257	0.033	0.152	0.211
90	189	0.047	0.033	193	0.256	0.033	0.152	0.209
100	167	0.047	0.032	171	0.255	0.031	0.151	0.208

[a] E_m represents the midpoint potential measured as $(E_p^{red} + E_p^{ox})/2$ in volts versus Ag/AgCl(3 M KCl). E_p^{red} and E_p^{ox} are reduction and oxidation peak potentials, respectively; Q_{red} and Q_{ox} are the charges associated with the reduction and oxidation components; $W_{1/2}{}^{red}$ and $W_{1/2}{}^{ox}$ are the peak widths at half-height for the reduction and oxidation components, respectively. Data reported are for every 10 cycles.

Table 2. Voltammetric Parameters Obtained at Scan Rate of 0.02 V s^{-1} When TCNQ Microcrystals Immobilized by Drop Casting onto Four Different Electrode Materials Are Placed in Contact with 0.1 M $Co(ClO_4)_{2(aq)}$[a,b]

electrode material	area (cm^2)	E_p^{red} (V)	$W_{1/2}{}^{red}$ (V)	E_p^{ox} (V)	$W_{1/2}{}^{ox}$ (V)	E_m[c] (V)	ΔE_p^{ox-red} (V)
GC	0.070	0.037	0.045	0.265	0.027	0.151	0.221
Pt	0.020	0.036	0.041	0.264	0.029	0.150	0.221
Au	0.020	0.041	0.044	0.262	0.026	0.151	0.214
ITO	0.090	0.016	0.062	0.282	0.074	0.149	0.266

[a] Voltammetric data presented obtained after five cycles of the potential. [b] Symbols in headings are defined in Table 1. [c] The error associated with E_m values is ±3 mV.

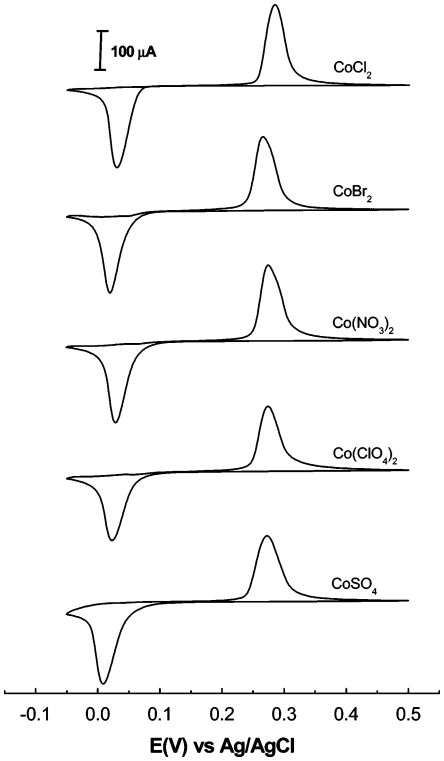

Figure 2. Cyclic voltammograms of TCNQ microcrystals immobilized via mechanical attachment onto a 3 mm GC electrode (scan rate 0.02 V s^{-1}) in contact with 0.1 M aqueous solutions of $CoCl_2 \cdot 6H_2O$, $CoBr_2 \cdot H_2O$, $Co(NO_3)_2 \cdot 6H_2O$, $Co(ClO_4)_2 \cdot 6H_2O$, and $CoSO_4 \cdot 7H_2O$. The currents are normalized to the peak heights for comparison purposes.

Table 3. Voltammetric Parameters Obtained at a Scan Rate of 0.02 V s^{-1} for TCNQ Microcrystals Immobilized on a 3 mm Diameter GC Electrode (Mechanical Attachment) When Immersed in a 0.1 M $Co^{2+}_{(aq)}$ Solution of Different Anions[a]

electrode material	E_p^{red} (V)	$W_{1/2}^{red}$ (V)	E_p^{ox} (V)	$W_{1/2}^{ox}$ (V)	E_m (V)	ΔE_p^{ox-red} (V)	Q_{red}[b] (μC)
$CoCl_2 \cdot 6H_2O$	0.029	0.032	0.284	0.035	0.156	0.255	408
$CoBr_2 \cdot H_2O$	0.019	0.031	0.265	0.037	0.142	0.246	327
$Co(NO_3)_2 \cdot 6H_2O$	0.028	0.033	0.275	0.039	0.152	0.246	269
$Co(ClO_4)_2 \cdot 6H_2O$	0.024	0.036	0.276	0.037	0.150	0.252	334
$CoSO_4 \cdot 7H_2O$	0.011	0.026	0.270	0.043	0.141	0.258	265

[a] Voltammetric data obtained after five cycles of potential over the range from 0.5 to − 0.05 V. Symbols in headings are defined in Table 1. [b] The differences in the charge are due to different masses of TCNQ-modified GC electrode together with the different dissolution rate of the generated $Co[TCNQ]_2(H_2O)_2$ materials.

is observed, probably due in large part to ohmic distortion from the high level of uncompensated resistance present at low electrolyte concentrations. The inert zone width, ΔE_p^{ox-red}, increases gradually from 0.213 V at 1.0 M to 0.339 V at 0.001 M, which may be also attributed to the uncompensated resistance effects encountered as the $Co^{2+}_{(aq)}$ electrolyte concentration decreases.

If the overpotentials associated with the oxidation (E_p^{ox}) and reduction (E_p^{red}) processes are equal, the midpoint potential, E_m, would represent the reversible potential (E_R), ($E_R = (E_p^{ox} + E_p^{red})/2$, so that E_m would depend on the concentration of $Co^{2+}_{(aq)}$ in a Nernstian manner.[22] Thus, an E_m shift of ca. 30 mV per decade change in concentration is expected if the activity of the reduced and oxidized solid phases is equal to unity. The dependencies of E_p^{ox}, E_p^{red}, and E_m on log [Co^{2+}] are plotted in Figure 3b, and data are summarized in Table 4. E_m shifts from 0.191 to 0.098 V

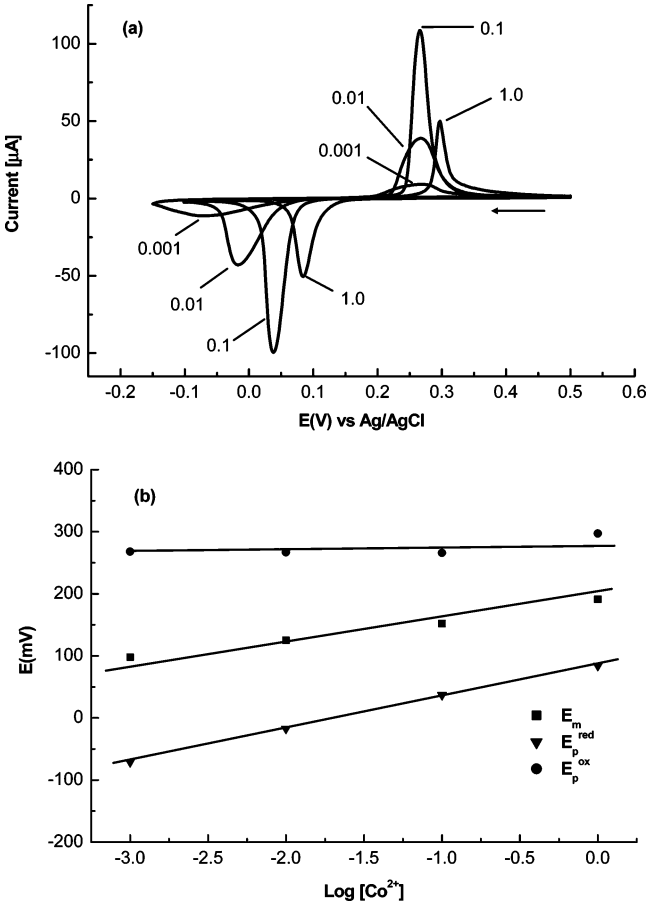

Figure 3. (a) Cyclic voltammograms obtained under steady-state conditions (fifth cycle shown) from a TCNQ-modified GC electrode (mechanical attachment) immersed in aqueous $Co(ClO_4)_2$(aq) electrolyte at designated concentration and a scan rate of 0.01 V s^{-1}. (b) Dependence of E_p^{ox}, E_p^{red}, and E_m on $Co^{2+}_{(aq)}$ concentration.

Table 4. Voltammetric Data Obtained at a Scan Rate of 0.01 V s^{-1} with a TCNQ-Modified GC Electrode (Mechanical Attachment) Immersed in Different Concentrations of $Co(ClO_4)_2 \cdot 6H_2O_{(aq)}$ Solution[a]

$[Co^{2+}_{(aq)}]$ (M)	E_p^{red} (V)	$W_{1/2}^{red}$ (V)	E_p^{ox} (V)	$W_{1/2}^{ox}$ (V)	E_m (V)	ΔE_p^{ox-red} (V)	Q_{red}[b] (μC)
1.0	0.084	0.028	0.297	0.018	0.191	0.213	216
0.1	0.037	0.030	0.266	0.027	0.152	0.229	348
0.01	−0.017	0.055	0.267	0.057	0.125	0.284	284
0.001	−0.071	0.142	0.268	0.084	0.098	0.339	149

[a] Voltammetric data obtained after five cycles over the potential range from 0.5 to −0.05 V. Symbols in headings are defined in Table 1. [b] The differences in the charge result from differences in both $Co^{2+}_{(aq)}$ concentrations and masses of TCNQ adhered to the GC electrode.

when the $Co^{2+}_{(aq)}$ concentration changes from 1.0 M to 1.0 mM. The direction of the potential change and the 93 mV total shift or 31 mV per decade change in concentration are as anticipated for a Nernstian or reversible process assuming a two-electron charge-transfer process.

I.E. Probing the Nucleation and Growth Process of $Co[TCNQ]_2(H_2O)_2$. (a) Scan Rate Effect. Inspection of representative cyclic voltammograms illustrated in Figure 4a as a function of scan rate and data in Table 5 demonstrate that E_p^{red} becomes less positive as the scan rate is increased (55 mV shift in E_p^{red} in changing the scan rate from 0.005 to 0.1 V s^{-1}). This scan rate dependence is as expected for a nucleation−growth-type process.[37] In contrast, only a 24 mV shift is obtained for the oxidation counterpart, E_p^{ox},

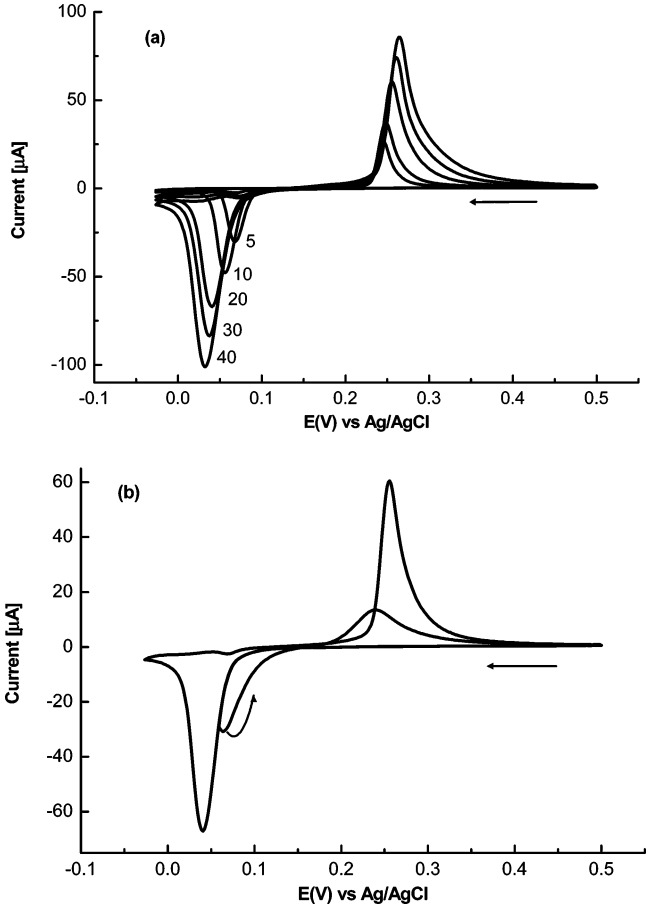

Figure 4. (a) Cyclic voltammograms of TCNQ-modified GC electrode (mechanical attachment) in contact with 0.1 M $Co(ClO_4)_{2(aq)}$ solution at designated scan rates. (b) Cyclic voltammograms obtained under the same condition as part a and a scan rate of 0.020 V s^{-1}. Fourth cycle shown followed by the fifth cycle when the potential is switched at the foot of the reduction wave, which induces a hysteresis loop into the voltammogram, as indicated by the arrows.

Table 5. Voltammetric Data Obtained as a Function of Scan Rate for TCNQ-Modified GC Electrode (Mechanical Attachment) Placed in Contact with 0.1 M $Co(ClO_4)_2 \cdot 6H_2O_{(aq)}$ Solution[a]

scan rate (V s^{-1})	E_p^{red} (V)	$W_{1/2}^{red}$ (V)	E_p^{ox} (V)	$W_{1/2}^{ox}$ (V)	E_m (V)	ΔE_p^{ox-red} (V)
0.005	0.068	0.022	0.245	0.020	0.156	0.177
0.010	0.056	0.024	0.248	0.024	0.152	0.192
0.020	0.040	0.030	0.255	0.029	0.147	0.215
0.030	0.037	0.032	0.260	0.030	0.148	0.223
0.040	0.032	0.035	0.264	0.034	0.148	0.232
0.050	0.023	0.040	0.268	0.040	0.145	0.245
0.100	0.013	0.051	0.269	0.064	0.141	0.256

[a] Voltammetric data collected after five potential cycles. Symbols in headings are defined in Table 1.

thereby indicating that the scan rate effect is more prominent for the reduction process. Significant increases in both $W_{1/2}$ and ΔE_p also are detected at higher scan rates. In contrast to the result expected for a thermodynamically significant parameter, the midpoint potential, E_m, is slightly affected by changing the scan rate. Additional support for the presence of a nucleation and growth process is obtained from voltammetric scans switched at the onset of the reduction process. For example, in Figure 4b, for the fifth cycle of the potential, when the potential was switched at 0.06 V, which corresponds to the foot of the reduction process, a current loop is produced (having a zero current crossover potential around 0.160 V) which is highly characteristic of processes involving nucleation−growth kinetics.[26,37]

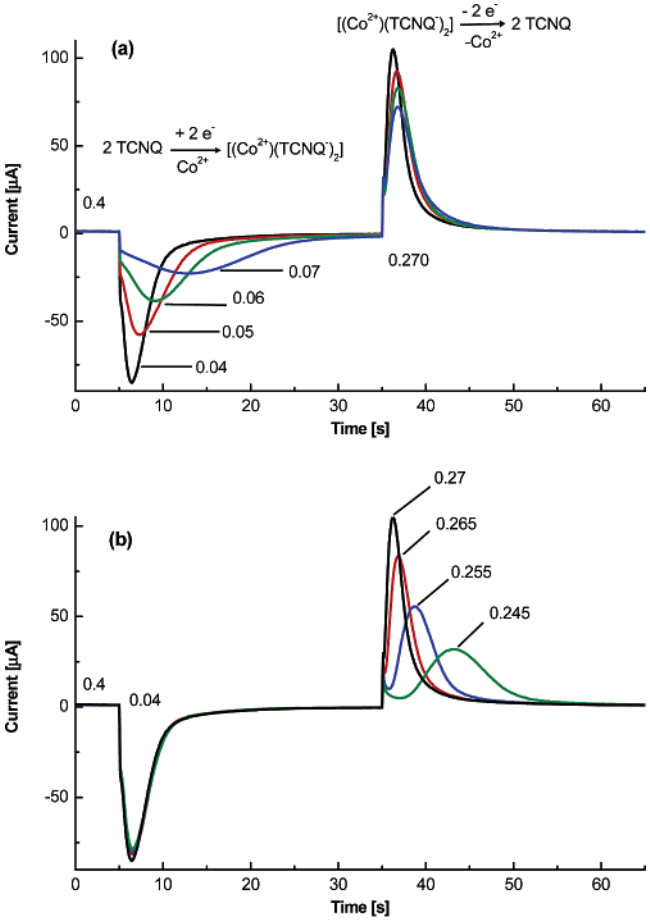

Figure 5. Double-potential step chronoamperograms obtained when a 3 mm diameter GC electrode modified with microcrystals of TCNQ (mechanical attachment) is placed in contact with 0.1 M $Co(ClO_4)_2 \cdot 6H_2O_{(aq)}$. (a) $I-t$ curves obtained when the potential is stepped from 0.40 to 0.040, 0.050, 0.060, and 0.070 V to induce reduction and then back to 0.270 V in each case to induce oxidation. (b) $I-t$ curves obtained when the potential is stepped from 0.40 to 0.040 V to induce reduction and then back to 0.270, 0.265, 0.255, and 0.245 V. The peaks in the current−time transients are indicative of nucleation−growth kinetics.

(b) Chronoamperometry. Even more definitive evidence for a nucleation-growth process is provided by double potential step chronoamperometric (DPSCA) experiments.[37−39] Figure 5 illustrates the results of a series of DPSCA measurements performed on a TCNQ-modified GC electrode which had been subjected to one potential cycle at a scan rate of 0.020 V s^{-1} over the potential range from 0.4 to −0.05 V.[41] The initial step (30 s) is to a potential that allows reduction of TCNQ to $[TCNQ]^-$ to occur with concomitant formation of the corresponding $Co[TCNQ]_2$-based material, while the second step reverses this process by oxidation at similar step duration. After each potential step the current−time transient shows the expected charging current spike, which rapidly decays toward zero followed by the appearance of a well-defined faradaic current response. The faradaic component of the current−time transients then increases before decaying to zero (see Figure 5a,b) as expected for nucleation and growth kinetics.[42]

(41) This procedure was performed to reduce the size of the TCNQ crystals, which were freshly adhered to the GC electrode, thereby resulting in reproducible data.

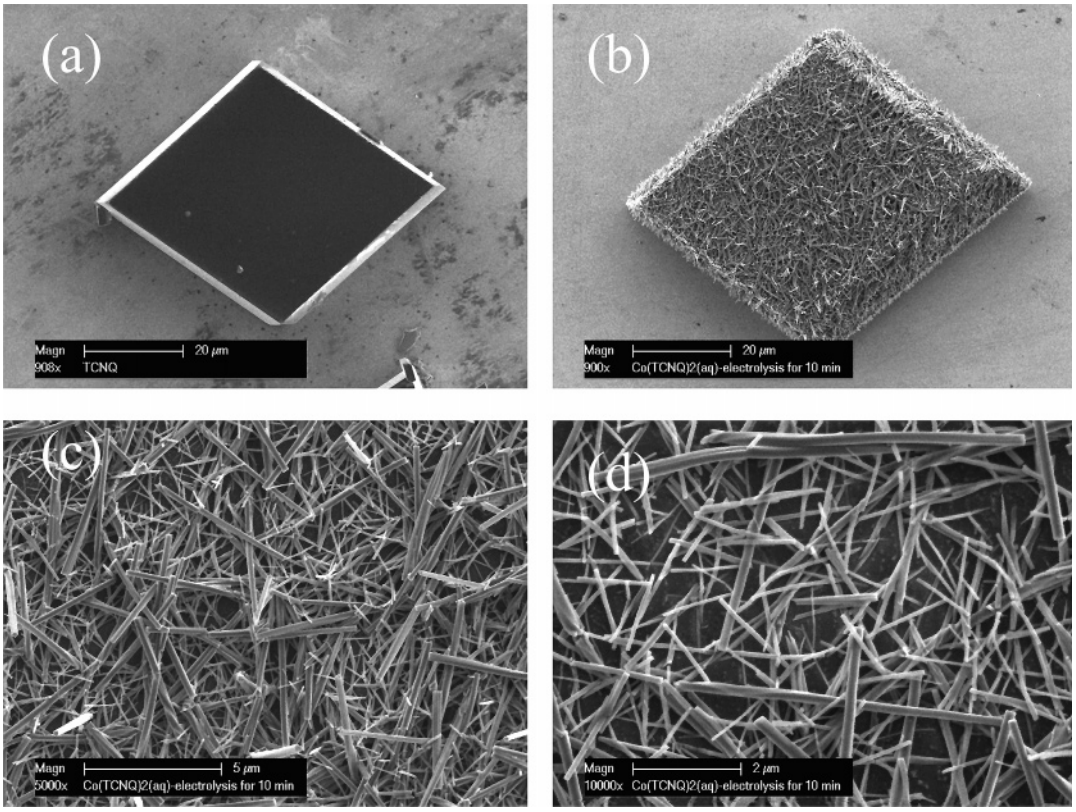

Figure 6. (a) SEM image of a TCNQ-modified ITO electrode prepared via the drop-cast method. (b) SEM image of $Co[TCNQ]_2(H_2O)_2$ formed by reductive electrolysis for 10 min at −0.05 V of TCNQ immobilized on an ITO electrode as in part a in contact with 0.1 M $Co(NO_3)_2{\cdot}6H_2O_{(aq)}$ electrolyte. (c and d) Same as for part b but at higher magnifications.

Table 6: Summary of Infrared Absorption Frequencies for $Co[TCNQ]_2(H_2O)_2$ Materials Prepared Chemically and Electrochemically

method of preparation	δ(C−H) (cm^{-1})	ν(C═C), (cm^{-1})	ν(C≡N), (cm^{-1})
synthesis from $Co(NO_3)_2{\cdot}6H_2O$[a]	823 m	1505 s	2221 s, 2200 s, 2177 m
electrolysis[b]	824 m	1505 s	2218 s, 2203 s, 2178 m
cyclic voltammetry[c]	824 m	1506 s	2220 s, 2200 s, 2178 m

[a] From reaction of an aqueous solution of $Co(NO_3)_2{\cdot}6H_2O$ with LiTCNQ at 298 K and stirring for 30 min.[31] [b] Electrolysis at −0.05 V for 10 min of TCNQ-modified ITO electrode in the presence of 0.1 M $Co(ClO_4)_2{\cdot}6H_2O$. [c] After 40.5 cycles of scanning the potential from 0.5 to −0.05 V at a scan rate of 0.02 Vs^{-1} of mechanically attached TCNQ-modified ITO electrode.

II. Infrared Spectroscopic Characterization of $Co[TCNQ]_2(H_2O)_2$. TCNQ-modified GC or ITO electrodes in contact with 0.1 M $Co^{2+}_{(aq)}$ electrolyte were subjected to controlled potential electrolysis and cyclic voltammetric experiments followed by ex situ collection of IR spectra. In the case of ITO electrodes, visual inspection of the optically transparent surface revealed the transformation of yellow to blue solid, as expected if electrochemical conversion of the yellow TCNQ microcrystals into blue $Co[TCNQ]_2(H_2O)_2$ occurs.[31]

A comparison of IR data obtained for an authentic sample of $Co[TCNQ]_2(H_2O)_2$ and electrosynthesized samples (Table 6) confirms that electrochemical synthesis of $Co[TCNQ]_2(H_2O)_2$ has been achieved. Thus, regardless of the preparation method of $Co[TCNQ]_2(H_2O)_2$, three intense IR bands are found in the ν(C≡N) region (Table 6). These all have lower energies than that of the neutral TCNQ IR band (2222 cm^{-1}), thereby indicating the existence of reduced $[TCNQ]^-$ radical.[43] The sharp IR band at 1505 cm^{-1} also supports the presence of TCNQ in the reduced form.[33] Another informative region occurs in the 800−865 cm^{-1} range which gives rise to the δ(C−H) bend of TCNQ. Dunbar and co-workers used this region to detect the presence of the TCNQ ring-bending mode in the $[TCNQ{-}TCNQ]^{2-}$ σ-dimer[31] via a characteristic weak band at $\upsilon \leq 808$ cm^{-1}. The electrochemically produced $Co[TCNQ]_2(H_2O)_2$ materials show distinct δ(C−H) stretches at 823−824 cm^{-1}, consistent with the presence of the $[TCNQ]^-$ radical and not the $[TCNQ{-}TCNQ]^{2-}$ σ-dimer. Moreover, the observation of broad absorption IR bands at higher energy (3425 and 3344 cm^{-1}) together with a 1645 cm^{-1} band confirms the presence of coordinated water molecules in the electrochemically generated $Co[TCNQ]_2$-based material. An IR spectrum of $Co[TCNQ]_2(H_2O)_2$ formed as a result of 40.5 cycles of potential over the range from 0.5 to −0.05 V (conditions as for footnote c of Table 6) is provided in the Supporting Information (Figure SM2).

Taken together, the IR and electrochemical data imply that when microcrystalline TCNQ crystals are immobilized on the surface of an electrode and reduced in the presence of $Co^{2+}_{(aq)}$ electrolyte ions, $Co[TCNQ]_2(H_2O)_2$ is formed via a nucleation and growth mechanism according to the following equation.

$$2[TCNQ]_{(s)} + Co^{2+}{}_{(aq)} + 2e^- \overset{H_2O}{\rightleftharpoons} Co[(TCNQ)_2(H_2O)_2]_{(s)} \quad (5)$$

(42) Scaboo, K. M.; Chambers, J. Q. *Electrochim. Acta* **1998**, *43*, 3257.

(43) Khatkale, K. S.; Devlin, J. P. *J. Chem. Phys.* **1979**, *70*, 1851.

The fact that the reduction potential of (Co^{2+}/Co^0) is more negative than $TCNQ^0/[TCNQ]^{-,2-}$ reductions implies that $Co^{2+}_{(aq)}$ ions are involved in charge neutralization only and not the electron-transfer process. This situation is different from the CuTCNQ system, where $Cu^{2+}_{(aq)}$ ions participate in both processes.[26] However, as for the CuTCNQ formation, in the $Co^{2+}_{(aq)}$ case a drastic change in crystal size and morphology of parent TCNQ is expected upon conversion into $Co[TCNQ]_2(H_2O)_2$ material. These morphological changes along with the mechanistic aspects that accompany this chemically reversible solid−solid transformation have been probed by the SEM technique.

III. SEM Characterization of the TCNQ/$Co[TCNQ]_2(H_2O)_2$ Solid−Solid Redox Transformation. Figure 6 provides an electron micrograph of an approximately 40 × 40 μm single crystal of TCNQ formed on an ITO electrode via the drop-casting method before (Figure 6a) and after (Figure 6b−d) 10 min of reductive electrolysis at $E_{app} = -0.05$ V vs Ag/AgCl when the electrode is placed in contact with a 0.1 M aqueous solution of $Co(NO_3)_2 \cdot 6H_2O$ electrolyte. Interestingly, after electrolysis, the surface of the parent TCNQ crystal is covered with small needle-shaped crystals that are associated with the transformation by reduction into $Co[TCNQ]_2(H_2O)_2$. Inspection at higher magnifications (Figure 6c and d) reveals the presence of straight needles (nanowires or nanorods) having diameters of 100−200 nm and lengths of 4−6 μm. Thus, while the overall rhombus shape of the TCNQ crystal remains intact, blue solid needle-shaped $Co[TCNQ]_2(H_2O)_2$ formed by this reductive electrolysis of the surface of the TCNQ crystal are generated. Presumably, the large size of the parent TCNQ crystal inhibits $Co[TCNQ]_2(H_2O)_2$ growth through the center of the crystal. EDAX analysis of the blue crystalline material confirmed the presence of cobalt along with carbon and nitrogen.

This finding, that $Co[TCNQ]_2(H_2O)_2$ crystals are formed on the edges and top of large TCNQ crystals, raises the question of the nature and location of the nucleation sites associated with the electrochemically generated $Co[TCNQ]_2$-based material and the growth process. From an energetic point of view, the most likely location for formation of nuclei would be the triple solid|electrode|electrolyte interface.[38] Thus, $Co[TCNQ]_2(H_2O)_2$ crystals probably grow from nuclei formed at the base of the TCNQ crystal with the faster rate being along the edges. This 'networklike' nucleation and growth mechanism is most likely facilitated by the semiconducting nature of the $Co[TCNQ]_2$-based materials.[17,30,33]

The mechanical attachment method provides an electrode surface with more densely packed and smaller sized TCNQ particles (see Figure 7a). Reductive electrolysis experiments at ITO surfaces modified in this manner give rise to a dramatic difference in morphology when the parent TCNQ crystals (Figure 7a) are converted to $Co[TCNQ]_2(H_2O)_2$ material (Figure 7b,c) relative to the situation described when using the drop-casting method. In this case, arrays of closely packed nanorods are generated. As can be seen in Figure 7c, at higher magnification most of the $Co[TCNQ]_2(H_2O)_2$ nanorods grow outward from the original TCNQ layer. These nanorods have an almost uniform diameter (~100 nm).

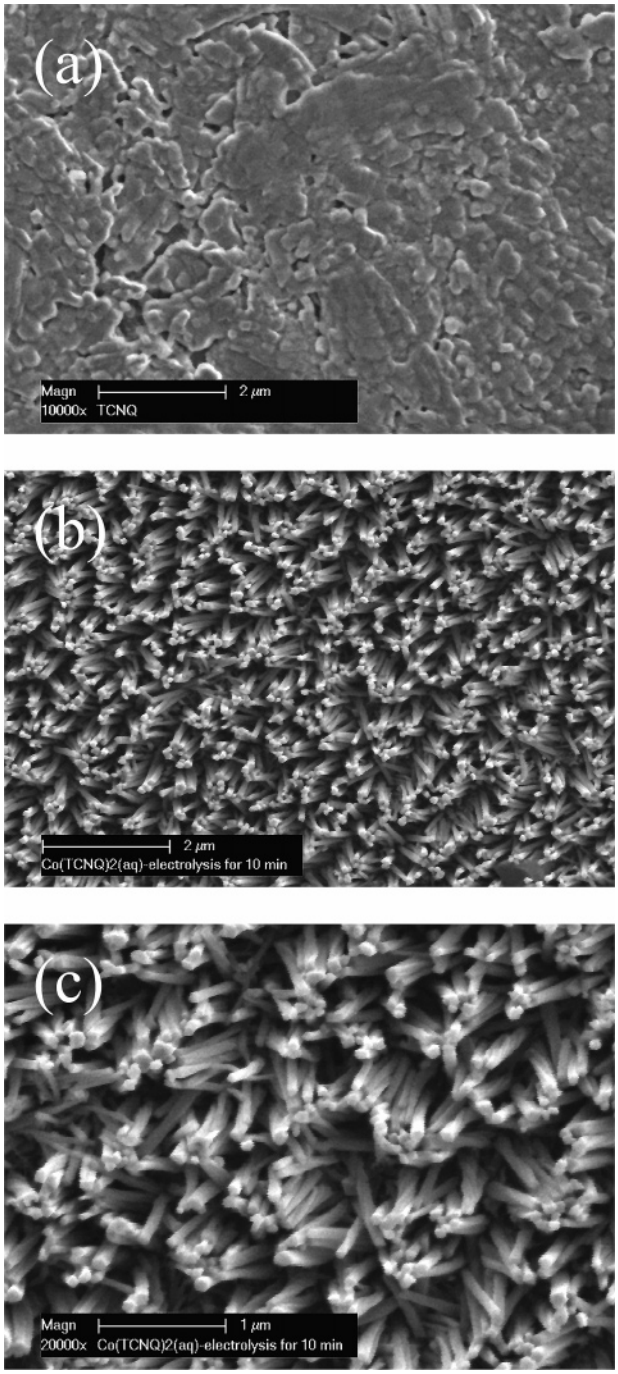

Figure 7. (a) SEM images of an ITO electrode modified via mechanical attachment method with solid TCNQ. (b) SEM image (at same magnification) of $Co[TCNQ]_2(H_2O)_2$ formed by reductive electrolysis of TCNQ adhered to an ITO electrode in the presence of 0.1 M $Co(NO_3)_2 \cdot 6H_2O$ for 10 min at −0.05 V. (c) Same as image b but at higher magnification.

Clearly, the method of electrode modification plays an important role in controlling the size and morphology of the parent TCNQ and hence the electrochemically generated $Co[TCNQ]_2(H_2O)_2$ crystals.

Figure 8 provides SEM images obtained after TCNQ microcrystals adhered to an ITO surface (via mechanical attachment) are placed in contact with a solution of 0.1 M $Co^{2+}_{(aq)}$ electrolyte and subjected to 40.5 cycles of potential over the range from 0.5 to −0.05 V. Clearly, the morphology of the solid generated under conditions of cyclic voltammetry differs from that formed when bulk electrolysis is used. A high level of transformation of TCNQ particles into needle-

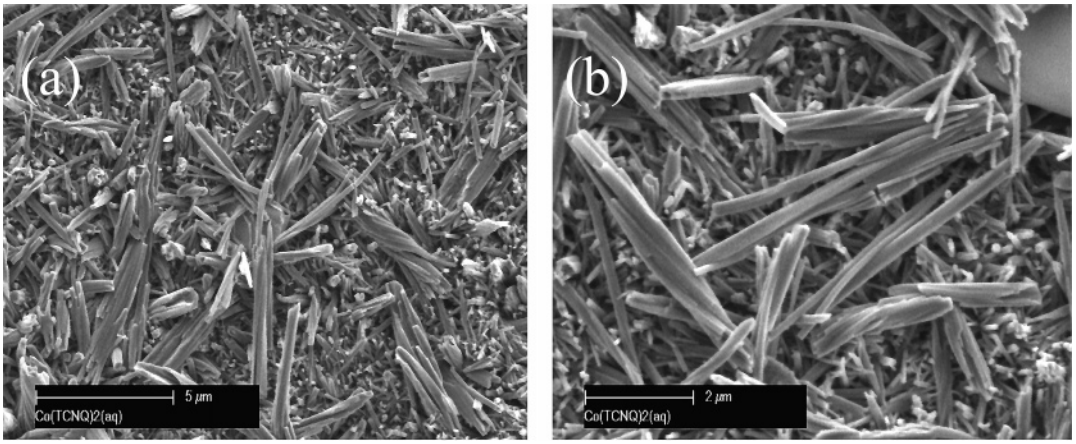

Figure 8. SEM images at different magnifications obtained after completion of 40.5 potential cycles (0.5 to −0.05 V) when an ITO electrode modified via mechanical attachment with solid TCNQ is placed in contact with 0.1 M $Co(NO_3)_2 \cdot 6H_2O_{(aq)}$ electrolyte.

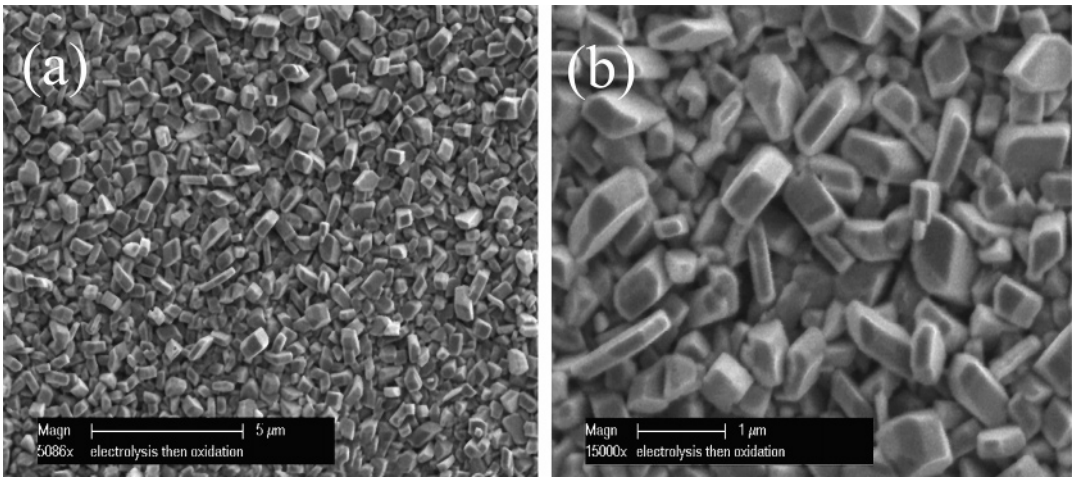

Figure 9. SEM images at low (a) and high (b) magnifications showing the morphology of microcrystals of TCNQ formed after a sequence of reductive electrolysis of TCNQ immobilized on ITO surface (mechanical attachment) at $E_{app} = -0.05$ V to form $Co[TCNQ]_2(H_2O)_2$, followed by oxidative electrolysis back to TCNQ at $E_{app} = 0.4$ V for 10 min. The well-defined pattern of cubic/rhombus-shaped microcrystals of TCNQ formed by this reduction−oxidation sequence should be compared with the TCNQ morphology present prior to electrolysis (Figure 7a).

shaped $Co[TCNQ]_2(H_2O)_2$ is detected, and some of these crystals now have lengths of 3−5 μm with outgrowths and twisting being observed in some of them (see Figure 8a and b). The changes in crystal shape and size associated with repetitive potential cycling experiments may be attributed to the chemically reversible solid−solid redox conversion sequence $Co[TCNQ]_2 \rightleftharpoons$ TCNQ. In each reductive stage the rhombus TCNQ crystals are converted to $Co[TCNQ]_2(H_2O)_2$ needles by incorporation of $Co^{2+}_{(aq)}$ ions. Upon oxidation, smaller TCNQ particles are formed than initially present, ultimately leading to smaller sizes of solid TCNQ particles being utilized in $Co[TCNQ]_2(H_2O)_2$/TCNQ transformation.

Reversible transformation of TCNQ and $Co[TCNQ]_2(H_2O)_2$ was also monitored by SEM under conditions of controlled potential electrolysis. If a modified electrode prepared by mechanical attachment of TCNQ is immersed in a 0.1 M solution of $Co^{2+}_{(aq)}$ electrolyte and reductive electrolysis is performed at −0.05 V, then blue $Co[TCNQ]_2(H_2O)_2$ material is generated from the initially compact yellow TCNQ layer. Oxidation of this solid at 0.4 V reveals a rapid color change from blue to yellow in the first 2 min of electrolysis, as expected if exclusion of $Co^{2+}_{(aq)}$ ions from the crystal lattice occurs to regenerate neutral TCNQ. SEM images obtained after 10 min of oxidation (Figure 9) explicitly show the presence of dispersed small cubic/rhombus-shaped TCNQ crystals, which are clearly distinguished (Figure 9b) from the nanorod-shaped $Co[TCNQ]_2(H_2O)_2$ material generated in the reduction step (Figure 7c) and the parent TCNQ layer (Figure 7a). Thus, TCNQ crystals fragment and decrease in size to accommodate the different morphologies of the TCNQ and $Co[TCNQ]_2(H_2O)_2$ forms during the rhombus−needle−rhombus reduction−oxidation sequence. IR characterization of the yellow solid revealed the presence of three characteristic IR bands at 2222 (s), 1542 (s), and 860 (s), thereby confirming regeneration of TCNQ.[43]

IV. Powder X-ray Diffraction of $Co[TCNQ]_2(H_2O)_2$. XRD powder patterns of a TCNQ-modified ITO electrode obtained prior to electrochemical experiments and electrochemically synthesized $Co[TCNQ]_2$-based material formed after 30 min of reductive electrolysis at −0.1 V vs Ag/AgCl are shown in Figure 10. Although the diffraction peaks of unreacted TCNQ and ITO can still be detected after electrolysis and the former are probably enhanced due to preferred orientation, the complete XRD powder pattern expected for $Co[TCNQ]_2(H_2O)_2$ was detected. That is, diffraction peaks observed at 13.83°, 15.47°, 19.59°, 21.94°, 25.05°, 31.19°, and 41.03° closely match those reported by Dunbar and co-workers[31] for chemically synthesized

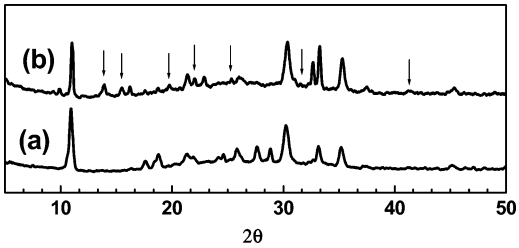

Figure 10. XRD powder patterns for a TCNQ-modified ITO electrode (a) before and (b) after being in contact with 0.1 M $Co(ClO_4)_2$ under reductive electrolysis conditions of $E_{app} = -0.1$ V vs Ag/AgCl for 30 min. Arrows refer to peaks identified as being associated with electrochemically generated $Co[TCNQ]_2(H_2O)_2$.

$Co[TCNQ]_2(H_2O)_2$. Therefore, the XRD data confirm that the electrochemically formed product is $Co[TCNQ]_2(H_2O)_2$ and that it is in a crystalline state.

Mechanistic Aspects of $Co[TCNQ]_2(H_2O)_2$ Formation. Voltammetric, spectroscopic, and microscopic data demonstrate that when rhombus-shaped TCNQ immobilized on an electrode surface is reduced by a single electron process to the monoanion radical, $[TCNQ]^-$, in the presence of $Co^{2+}_{(aq)}$-containing electrolyte, the corresponding needle-shaped blue solid $Co[TCNQ]_2(H_2O)_2$ is formed via an overall two-electron charge-transfer process (eq 6) by a nucleation and growth mechanism.

$$2[TCNQ]_{(s)} + Co^{2+}_{(aq)} + 2e^- + 2H_2O \rightleftharpoons Co[(TCNQ)_2(H_2O)_2]_{(s)} \quad (6)$$

$Co[(TCNQ]_2(H_2O)_2$ is most likely formed via a transitional $Co[TCNQ]_2$ intermediate (eqs 7 and 8). The latter is presumably formed via transport of $Co^{2+}_{(aq)}$ ions across the TCNQ aqueous|solid interface in the region where direct contact of immobilized $TCNQ_{(s)}$ and electrode surface occurs, and hence reduction takes place. Solvation to afford the thermodynamically favored $Co[(TCNQ]_2(H_2O)_2$ solid rapidly follows.

$$2[TCNQ]_{(s)} + Co^{2+}_{(aq)} + 2e^- \rightleftharpoons Co[(TCNQ)_2]_{(s)} \quad (7)$$

$$Co[(TCNQ)_2]_{(s)} + 2H_2O \rightarrow Co[(TCNQ)_2(H_2O)_2]_{(s)} \quad (8)$$

Conclusion

The chemically reversible solid−solid-phase transformation of a TCNQ-modified electrode in the presence of $Co^{2+}_{(aq)}$ electrolytes, induced by electrochemical methods, allows generation of blue crystalline needles or nanorods of $Co[TCNQ]_2(H_2O)_2$ material via an overall two-electron charge-transfer process with a nucleation and growth rate-determining step. In voltammetric experiments, regimes characterized by symmetrical reduction and oxidation processes along with large inert zones (0.23 V) are obtained. Generally, the voltammetric behavior is almost independent of electrode material and identity of cobalt electrolyte anion but displays marked dependence on electrolyte concentration, scan rate, and method of electrode modification. Formation of $Co[TCNQ]_2(H_2O)_2$ material was monitored by a variety of voltammetric techniques, and its structure and morphology were identified using IR spectroscopy, XRD, and scanning electron microscopy.

The method of electrode modification, drop casting or mechanical attachment, gave rise to different voltammetry, which is associated with the different particle sizes of the adhered TCNQ crystals. SEM monitoring of the change in crystal morphology in going from TCNQ to $Co[TCNQ]_2(H_2O)_2$ and back to TCNQ via a reductive−oxidative electrolysis pathway establishes the chemically reversible nature of the solid−solid-phase transformation as the regenerated smaller sized TCNQ crystals still display their normal cubic/rhombus shape after this redox-based electrolysis sequence. These results underscore the importance of the methodologies of surface immobilization on the voltammetry of $Co[TCNQ]_2$-based materials and highlight their role in controlling the morphology and particle size of the parent TCNQ as well as the electrochemically generated cobalt-containing crystals.

Acknowledgment. The authors express their appreciation to Alex Bilyk, Steven Pentinakis, and John Ward at the CSIRO division of Manufacturing, Infrastructure and Technology (CMIT) for technical assistance in obtaining SEM images. Financial support from the Australian Research Council also is gratefully acknowledged.

Supporting Information Available: Two figures showing cyclic voltammograms of TCNQ microcrystals immobilized via the drop-cast method onto four different electrode surfaces when placed in contact with 0.1 M $Co^{2+}_{(aq)}$ electrolyte (SM1) and IR spectra of $Co[TCNQ]_2(H_2O)_2$ formed as a result of 40.5 potential cycles over the range from 0.05 to −0.5 V when a TCNQ-modified ITO electrode is immersed in 0.1 M $Co^{2+}_{(aq)}$ electrolyte (SM2). This material is available free of charge via the Internet at http://pubs.acs.org.

CM060852J